

Quantifying the Impact of Ecosystem Services for Landscape Management under Wildfire Hazard

3 Pelagie Elimbi Moudio · Cristobal Pais · Zuo-Jun

4 Max Shen

5

6 Received: date / Accepted: date

7 Abstract In recent years, the frequency, intensity, and severity of wildfires are on the rise
8 due to various environmental factors. Several studies show that the strategic application of
9 fuel treatments are effective at altering fire behavior and its spread patterns. Effective plan-
10 ning for mitigating future expected losses under wildfire risk is a complex challenge that
11 requires the integration of fire spread, simulation, and optimization models as well as the
12 inclusion of multiple objectives into a unified framework. Previous works simplify the anal-
13 ysis by valuing the landscape regions using a unique objective (e.g., minimize the average
14 expected area burned) or a predefined objective function. However, such an assumption is
15 a simplification of the real system as multiple parts of the landscape have different values
16 based on factors such as the presence of human settlements and infrastructure, availability
17 of environmental services, and forest health, among others. In this work, we expand these
18 previous attempts by providing an integrated framework to naturally include and weight
19 multiple objectives into the optimization model and analyze the trade-off between present
20 objectives and future protection against wildfire risk. We study three key regions based on
21 their recent fire history, landscape diversity, and demographic variety to quantify the impact
22 of multiple objectives in landscape management. We obtain treatment plans using various
23 combinations of these layers reflecting how different priorities of the decision-makers could
24 affect treatment policies.

25 Keywords Wildfire risk analysis · Disaster management · Natural hazard · Decision-making
26 under uncertainty · Fire risk · Fire-resilient landscapes

Pelagie Elimbi Moudio

Industrial Engineering and Operations Research Dept., University of California, Berkeley, 94720 CA, USA

Tel.: +1-617-710-3983

ORCID(s): 0000-0002-1221-0529

E-mail: pelagy.elimbimoudio@berkeley.edu

Cristobal Pais

Industrial Engineering and Operations Research Dept., University of California, Berkeley, 94720 CA,
USA

ORCID(s): 0000-0002-1392-5569

Zuo-Jun Max Shen

Industrial Engineering and Operations Research Dept., University of California, Berkeley, 94720 CA,
USA

27 1 Introduction

28 Evidence from multiple research areas suggests that the dehydrating effects of climate change
29 have caused a worldwide surge in the number and intensity of fires in the last decade and
30 these numbers are still soaring (Flannigan et al., 2009; Jolly et al., 2015; Williams and Abat-
31 zoglou, 2016; Abatzoglou and Williams, 2016; Running, 2006). These observations are fur-
32 ther highlighted when we note that some of the largest and devastating fires leading to heavy
33 human, financial, and infrastructural losses have occurred in the last decade. A closer look
34 at the state of California reveals that despite a decrease in the total number of fires within
35 the state, the total area burned by these fires has increased. In the last ten years, California
36 has been plagued by its most disastrous wildfires (Sun et al., 2019). The 2018 Camp Fire
37 is California's most destructive fire recorded, where a single fire destroyed more structures
38 than any other in modern history. This fire is also the most expensive natural disaster in
39 the world in 2018 in terms of insured losses resulting in the loss of 13,696 and the death
40 of over 88 people (Edwards, 2019; Baldassari, 2018; Fuller, 2018). Following in level of
41 destructiveness is the 2017 Tubbs Fire in the Napa and Sonoma counties, which destroyed
42 thousands of structures leading to 46 human fatalities (Geller, 2018; Nauslar et al., 2018). In
43 addition, human efforts in fire fighting are at maximum capacity. These factors suggest that
44 more preventative policies and measures must be taken beforehand to reduce the risk of fire
45 occurrence (Curt et al., 2016) at the Wild-land urban interface (WUI) and in large areas of
46 forest (Calviño-Cancela et al., 2016) to protect human lives and maintain an adequate coex-
47 istence with nature. In (Hirsch et al., 2001), researchers propose a paradigm that considers
48 opportunities in three main dimensions: i) decrease of the potential fire behavior of the land-
49 scape, ii) reduction of the potential impact of fire ignition, decreasing the expected losses
50 and number of escape wildfires in fire-prone areas, and iii) increase the capability of fire
51 suppression. The term Fire-Smart Forest Management (FSFM) has emerged and includes
52 the above concepts.

53 The strategic implementation of fuel treatment plans can alter and modify fire behavior
54 and aid in suppression efforts (Omi, 2015; Hirsch et al., 2001; Finney, 2001, 2004). These
55 fuel treatments consist of actions and procedures such as cutting and clearing wood, pre-
56 scribed burns, commercial harvesting, and thinning, that can promote fire hazard reduction
57 (Agee and Skinner, 2005). In (Salis et al., 2016), the authors discuss strategies to define
58 treatments using burning probability maps, the area burned, or the flame length. Other re-
59 search in this area focuses on finding the optimal spatial allocation of prescribed burning
60 activities (Alcasena et al., 2018; Matsypura et al., 2018), and designing fire breaks to con-
61 trol fire spreading (Russo et al., 2015).

62 The decision-makers that carry out these fuel treatments face questions about how to
63 make such decisions. However, the problem of optimal fuel allocation is challenging due to
64 various sources of uncertainties. In (Chung, 2015), the authors discuss challenges surround-
65 ing fuel treatment methods, timing, and the high uncertainty levels in climate and ignition
66 areas over multiple time periods. As a result, deterministic fire simulators such as FARSITE,
67 Prometheus, and Wildfire Analyst (Finney, 2004; Tymstra et al., 2010; Ramírez et al., 2011),
68 which can reproduce fires with and without treatment activities are popular in practice. The
69 main critique to using fuel treatment methods is that due to the difficulty in predicting wild-
70 fire occurrence and propagation, the allocation of these treatments generally do not match
71 areas in which future fires occur, leading to wasted investments coupled with economic,
72 human, and environmental losses (Barnett et al., 2016).

73 In order to address the mismatch between fuel treatment allocation and fire occurrence,
74 the authors in (Pais et al., 2019; Carrasco et al., 2019) develop a framework that integrates

75 fire spread, optimization, and simulation models. The study highlights an adaptable metric
76 known as the Downstream Protection Value (DPV), that ranks the impact of treating a unit
77 of the landscape, by modeling a forest as a network and the fire propagation as a tree graph.
78 The framework requires weather and topography inputs of the forest to run and can be
79 modified by users to incorporate region-specific forest data so as to provide more effective
80 and targeted treatments. Results from the first version of the model value the equivalent
81 volumes of subsets of the forest equally. However, such an assumption is limited in real
82 settings. Different parcels of a landscape may have different values based on multiple factors
83 such as the existence of animal migration corridors, the amount of biodiversity hosted in
84 that region, the presence of human settlements and infrastructure, or the amount of carbon
85 sequestered.

86 The main contribution of this study is extending the analysis on the integrated frame-
87 work proposed by (Pais et al., 2019) to aid decision making under wildfire uncertainty by
88 evaluating the sensitivity of the objective function to key environmental and economic fac-
89 tors. Three key regions in California (Napa Valley, Paradise, and Getty center) are chosen for
90 analysis based on the existence of documented catastrophic events in the last five years and
91 significant variance in vegetation types and demographic variables. We compare unweighted
92 treatment plans against versions including environmental and demographic factors such as
93 carbon sequestration, canopy height and density, population density, and accessibility of the
94 area, as well as expected future fire behavior. Using multiple combinations of these layers,
95 we generate different treatment plans that reflect how different priorities of the decision-
96 makers could affect the treatment policies. We then analyze the trade-off between maximiz-
97 ing the decision-maker utility function and protecting the land against future expected losses
98 due to wildfire with the aim of finding robust treatment plans.

99 **2 Material and Methods**

100 **2.1 Data Extraction and Processing**

101 The California region with its established seasonal fires is the focus region in our study
102 because of the existence of documented and destructive fire events. The default framework
103 relies on weather and topographic data obtained from various sources. In addition, we dis-
104 cuss how to generate the main layers that serve as weights for estimating the risk associated
105 with each unit of landscape in our optimization module. We group the layers extracted for
106 the objective function into Environmental factors (e.g., canopy density/height) and Demo-
107 graphic characteristics (e.g., population density, accessibility). Additionally, we split the
108 data into a training and test set. During training, we fine-tune key parameters in our model
109 using the training data set. The test set allows us to measure the performance of our model
110 by assessing how well our model results compare to real data.

111 The data consists of a combination of shapefiles and GeoTIFF files. For the most part,
112 these layers are already aligned and have the same resolution (30 x 30 m). We transform
113 the original data into a series of rasters to be ingested into our framework. Data enters
114 into the framework using two main approaches: (1) local data provided by the user and (2)
115 semi-automatic collection and processing of online assets (e.g., population density, climatic
116 conditions that can play a fundamental role in the propagation of the fire) available in Google
117 Earth Engine (GEE) (Gorelick et al., 2017), to easily generate a consolidated dataset (Fig.
118 1). This latter method relies on Python scripts and can be used as an independent module

119 for performing any kind of query in GEE. Finally, the data is automatically processed and
120 formatted to be ingested into the different modules of the proposed framework.

121 ***Environmental factors***

122 The building blocks for the data layers in this category are obtained from the Landscape
123 Fire and Resource Management Planning Tools (LANDFIRE) (Rollins, 2009) open reposi-
124 tory. This data hub consists of a shared program involving the participation of the U.S.
125 Department of Agriculture Forest Service and the U.S. Department of the Interior, provid-
126 ing support for fire and vegetation simulators created and used by the US Forest Service.
127 The Canopy bulk density (CBD) and the Canopy height (CH), each a grid with resolution
128 (30x30 m) are obtained directly from the database. CBD is a measure of the density of the
129 landscape canopy which is the portion of vegetation above ground. Canopy height as implied
130 by its name measures the height in meters of the landscape canopy.

131 ***Forest.*** We combine the CBD and CH layers in various manners to obtain the different
132 layers constituting the environmental factors category including estimating the area of green
133 vegetation in the forest (forest health) and carbon sequestration volume. The CBD and CH
134 layers are averaged together to form a new layer that serves as a proxy for forest health. The
135 CBD layer indicating vegetation density and the CH measuring vegetation height provide
136 insights about the health of the landscape vegetation.

137 ***Carbon Sequestration*** The carbon sequestration (CS) layer is estimated following the sim-
138 ple method proposed in (Foundation, 2002) for each unit in our landscape grid as follows:

1. Estimate the total (green) weight of the trees. Using the canopy density, we obtain the
canopy area by multiplying the density by the area of a unit cell. Then the canopy area is
multiplied by the canopy height to obtain a volume. Once we have the volume of green
in each cell, we use Huber's formula (Waddell, 1989) to estimate the weight using the
equation:

$$\text{Weight} = \text{volume} \times \text{green density}$$

139 where green density represents the total density of wood and bark combined (CBD).

- 140 2. According to previous research (DeWald et al., 2005), the average dry weight for differ-
141 ent temperate tree species in the United States is about 72.5% of regular weight. We use
142 these results to approximate the average dry weight of green for each cell.
- 143 3. Next, we estimate the weight of carbon using findings from (Birdsey, 1992), which state
144 that the carbon weight is about 50% of regular tree weight.
- 145 4. Finally, we calculate the average weight of carbon dioxide sequestered in the tree per
146 cell using:
 - 147 (a) The atomic weight of CO₂ is C + 2 × O = 43.999915.
 - 148 (b) The ratio of CO₂ to C is 43.999915/12.001115 = 3.6663

149 Therefore, to determine the weight of carbon dioxide sequestered in the tree, we multiply
150 the weight of carbon in the tree by a 3.6663 factor.

151 ***Fuel vegetation type.*** The fuel layer With a 30 by 30 m resolution that we require for our
152 simulations is obtained from the LANDFIRE (Rollins, 2009) publicly available repository¹.

¹ https://www.landfire.gov/bulk/downloadfile.php?FNAME=US_140_mosaic-US_140FBM40_20180618.zip&TYPE=landfire

153 It provides a categorical grid at a national level representing the forty Scott and Burgan fire
 154 behavior fuel models lastly updated in 2014. For a comprehensive analysis and description
 155 of all fuel types, their characteristics, and experimental parameters, see ([Scott, 2005](#)). State-
 156 level data (California) is locally extracted and uploaded into GEE to consolidate it with the
 157 additional layers of the study. This is the main input for calculating the fire rate of spread in
 158 the simulation model.

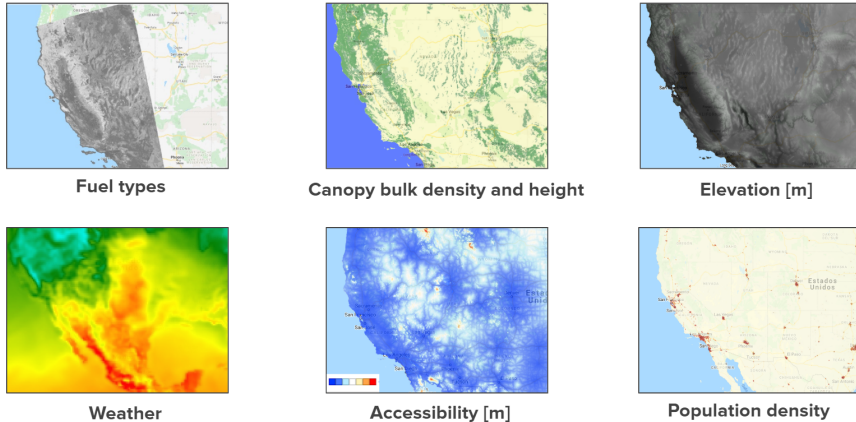


Figure 1: Example of layers included visualized in GEE. All layers are obtained for California and consolidated into a 30 by 30 m. multi-band raster.

159 **Weather and moisture scenarios.** The rate of Spread (ROS) mainly depends on the type
 160 of forest fuel that goes into combustion and the wind speed. However, another influencing
 161 factor is the moisture content of dead and live vegetation present in the forest. This variable
 162 is crucial for estimating the surface ROS as certain land-covers (e.g., grass types) tend to
 163 significantly modify their propagation patterns depending on their humidity levels. In order
 164 to capture and simulate interesting situations for the practitioners and researchers, multi-
 165 ple value thresholds are empirically studied. According to Scott & Burgan ([Scott, 2005](#)),
 166 these interesting humidity levels are represented by four scenarios: D1L1, D2L2, D3L3,
 167 and D4L4, from the driest (D1L1), where the fire tends to propagate faster, to the wettest
 168 (D4L4), with the opposite effect. Weather scenario files that describe the evolution of the
 169 temperature, wind speed, and wind direction are obtained from the historical time series of
 170 the closest weather station (with respect to the centroid of each instance) available for the
 171 simulated fire duration. Each fire is simulated for 12 hours under the D1L1 scenario, to be
 172 able to capture relevant propagation patterns.

173 **Demographics.** The estimated population densities (number of persons per square kilo-
 174 meter) for the years 2000, 2005, 2010, 2015, and 2020 are extracted from the Gridded
 175 Population of World Version 4 (GPWv4), Revision 11 dataset (<https://sedac.ciesin.columbia.edu/data/collection/gpw-v4>) at a resolution of 30 arc-second grid cell and
 176 averaged. Accessibility to cities, which measures the land-based travel time (minutes) to the
 177

nearest densely-populated areas with 1,500 or more inhabitants per square kilometer is obtained from the Malaria Atlas Project ([https://malariaatlas.org/research-project/
accessibility_to_cities/](https://malariaatlas.org/research-project/accessibility_to_cities/)) at a 30 second-arc resolution for 2015.

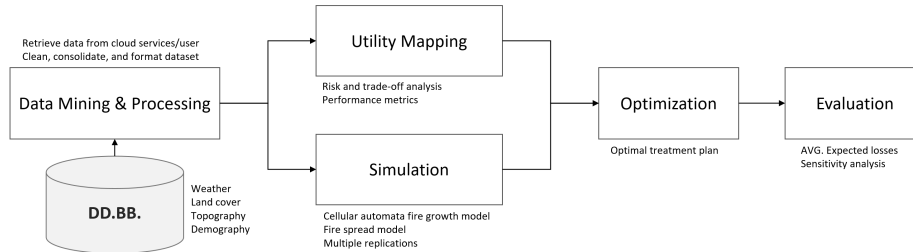


Figure 2: Framework schematic. Data is retrieved from cloud services and local user inputs. Decision-makers define relevant objectives by analyzing the trade-off between multiple variables. Once the data is processed, multiple simulations are performed to estimate the impact of future wildfires in the landscape. An optimization model is fed with the outputs from the utility mapping and simulation models. Finally, results are evaluated by estimating the average expected losses due to wildfire, as well as analyzing the sensitivity of the optimal treatment plan.

181 2.2 Wildfire simulation

182 A region of interest is modeled as a two-dimensional lattice with an underlying network
 183 structure to represent the connectivity between cells/nodes in the grid. Cells represent a ho-
 184 mogeneous area with similar characteristics, focusing on points of interest such as potential
 185 propagation sources, densely populated areas, natural reservoirs, among others. Each cell
 186 from the input data corresponds to a node in an undirected grid graph $G = (V, E)$. Nodes
 187 $i \in V$ is associated with relevant attributes (e.g., population density, fuel type) included as
 188 part of the risk evaluation and further optimization models. Nodes are connected by edges
 189 $e \in E$ with weights (the distance between cells) generated by the structure of the region. In
 190 the current version of the study, each cell has at most 8 neighbors to simplify the analysis of
 191 the framework. However, the model can be easily extended to a general case (graph) where
 192 nodes can be connected with any other in the lattice as long as they share information or are
 193 related by relevant variables for the model.

194 Adapting the simulation framework discussed in (Pais et al., 2019, 2020), the fire spreads
 195 following a messaging process between the cells of G . The intensity of these signals is
 196 represented by the rate of spread (ROS) obtained from an independent fire spread model
 197 (BEHAVE) integrated into the simulator (Burgan, 1984) that models the fire behavior for
 198 static conditions in the U.S. based on empirical studies. It is used to update the fire progress
 199 between neighboring cells at every time-step t . From here, a directed tree graph – denoted as
 200 *Propagation Tree* – is obtained, with a root at the ignition node i , $T_i = (V_i, E_i)$ where $V_i \subseteq V$
 201 contains the burned cells and E_i the directed edges representing the propagation trajectories
 202 of the fire within the region.

203 Simulator parameters may need calibration in order to reproduce realistic propagation
 204 patterns or capture the impact of previously unseen conditions. Multiple approximations

205 during the implementation of the spread models and inherent noise within the data may
 206 inaccurately represent the expansion of the fire. To account for this situation, we propose
 207 an automatic adjustment following the work in (Carrasco et al., 2019) of the main param-
 208 eters of the model via a hybrid AI-Optimization procedure that aims to minimize the dif-
 209 ferences between the simulated and historical fire scars of the region of interest. Using this
 210 approach, we can automatically adjust the ROS estimations to accurately represent observed
 211 fire perimeters. Therefore, decision-makers are able to automatically adjust the fire spread
 212 model to account for variations in the fire behavior and conditions of the area, obtaining
 213 more accurate simulation results.

214 **2.3 Risk analysis**

215 Relevant features are mapped onto a common scale and weighted to account for their relative
 216 importance for the decision-maker. In order to condense their information into a single utility
 217 function, each feature is mapped unto a common scale $[0, 1]$ using an adequate function
 218 (e.g., linear) according to the expected impact of the feature in the landscape. Thus creating
 219 a single matrix representing the original $n \times m$ grid containing the value for each node in
 220 landscape ($NV \in \mathbb{R}^{n \times m}$), different convex combinations of the relevant values-at-risk (raster
 221 layers) are utilized. Let $\mu_k \in [0, 1] \forall k \in K, \sum_{k \in K} \mu_k = 1$ with K being the total number of
 222 layers included in the study, we thus combine the layers as follows:

$$NV = \sum_{k \in K} \mu_k L_k \quad (1)$$

223 where $L_k \in \mathbb{R}^{n \times m}$ is the matrix of dimensions $n \times m$ containing the grid values of layer k .
 224 Following this framework, we obtain a consistent risk function across the entire graph. The
 225 detailed procedure is as follows:

- 226 1. Given a set of K features representing characteristics of the nodes, we map them into
 227 a common scale between $[0, 1]$. The mapping function (e.g., linear) from raw feature
 228 values to the $[0, 1]$ interval is selected by the researcher according to the impact of each
 229 feature in the construction of a global utility/cost function. For example, if the protection
 230 of nodes with higher population density is prioritized, an increasing non-linear function
 231 can be applied, where densely-populated nodes are associated with values near to one,
 232 while sparsely populated areas are mapped to near-zero values (see Fig. 3).
- 233 2. This procedure is repeated for all K features, obtaining a set of normalized variables.
- 234 3. Correlated and complementary variables are combined into meaningful categories by
 235 weighting individual features with weights. As an example, canopy bulk density and
 236 canopy height could be summarized into a *Forest* category that equally weights both
 237 variables. Similarly, accessibility and population density layers could be condensed into
 238 a *Demography* category.
- 239 4. Once all categories are generated and normalized, a global utility function is calculated
 240 repeating the weighting procedure.
- 241 5. Gaussian kernels are applied to smooth the distribution over the landscape/grid. This
 242 avoids abrupt changes in the utility function as well as accounts for the intrinsic corre-
 243 lation of the cells in the landscape dynamics (Fig. 6).

Using this framework, decision-makers are able to condense any number of features into unique values associated with each node of the graph (NV), as well as generate a series of scenarios to evaluate the impact of certain features and their weights. In this way, each node

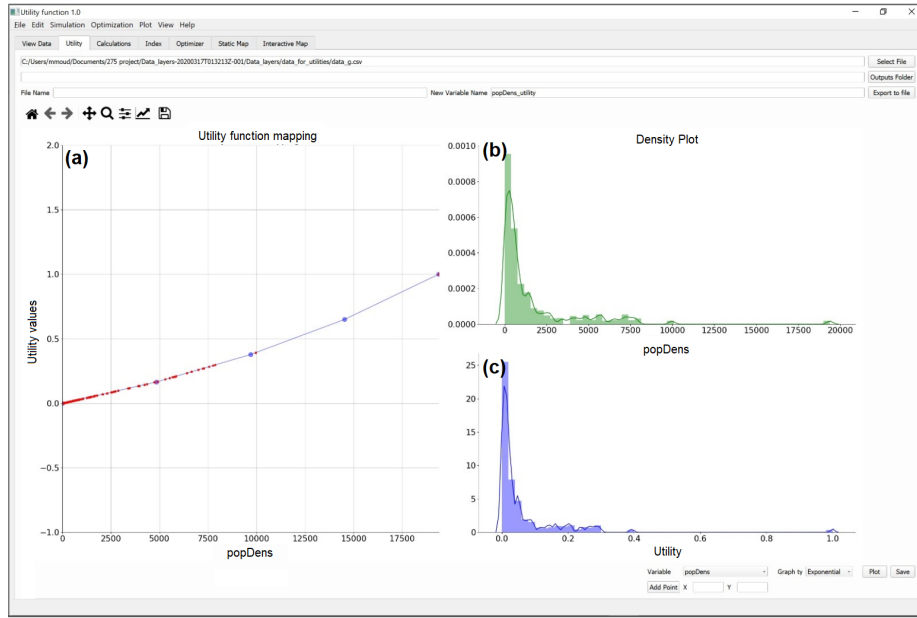


Figure 3: Utility mapper application. (a) The original values of the population density layer (x-axis, popDens) are mapped to the $[0,1]$ interval following an exponential function (y-axis). (b) Density plot for the original variable values. (c) Distribution of the mapped $[0,1]$ feature (called utility) following the applied transformation.

of the grid is characterized by a unique value incorporating all variables. Using different weight combinations allow us to control which factor we want to weight more in each instance (see Fig. 5). Next, we utilize the downstream-protection-value (*DPV*), a risk model that aims to measure the value of what is affected downstream in the network given the risk of a certain node (Pais et al., 2020). This model captures the role of a node in propagating the risk through the landscape based on the connectivity and relative influence of different nodes in the entire system. We define the *DPV* of node i inside the landscape network as:

$$\text{DPV}(i) = \alpha_i \sum_{j \in S_i} NV_j \quad (2)$$

where α_i is a weight factor for node i , e.g., the number of connections inside the region, allowing the prioritization and management of different zones; S_i is the set of nodes of the network that are affected by fire propagation from node i , and NV_j the value of node j incorporating all the relevant variables included to capture the potential losses caused by wildfire. Researchers can represent and evaluate multiple scenarios by providing different weights to the components of the risk function or to the final node value, thus obtaining variations of *DPV*. For example, NV values of nodes playing a fundamental role in the connectivity of the network could be weighted, among several options, by the degree of the node to highlight its importance in the propagation of fire. In addition, thanks to the nodes' additive property, there exists a natural extension from nodes to larger units (e.g., stands). This goes in hand with a practical implementation since authorities take decisions over certain areas with common characteristics instead of individual units, satisfying operational/logistic constraints.

256 2.4 An optimized resource allocation plan

257 Formulating an explicit optimization model (See Appendix, Section 4.1), we solve the prob-
258 lem of finding the connected cells that maximize the total utility/protection value considered
259 under wildfire risk, subject to specific constraints provided by the decision-maker (e.g., bud-
260 get). The connectivity constraints are imposed to mimic realistic scenarios where the protec-
261 tion of the landscape must be performed within connected patches to account for operational
262 constraints. If needed, these constraints can easily be relaxed by the decision-maker, running
263 a simplified version of the optimization model, or even implement his/her own algorithms.
264 In this way, we obtain an optimized treatment plan that identifies the set of units that, once
265 protected, will significantly disrupt the fire propagation while taking into account the impact
266 on relevant features of each node via the provided *NV* values.

267 We introduce $\lambda \in [0, 1]$ as the trade-off factor between the utility function defined by the
268 *NV* matrix and the DPV heatmap obtained after simulating *R* wildfires in the area. We de-
269 fine the objective function as the convex combination $U(\lambda) := \lambda DPV + (1 - \lambda)NV$, where
270 larger values of λ indicate that wildfire risk becomes more relevant to the decision-maker
271 when allocating resources through the network ($\lambda \rightarrow 1$) while smaller values represent the
272 case when the *NV* values play a more relevant role for prioritizing the treatments ($\lambda \rightarrow 0$).
273 Therefore, different optimized resource allocation plans are obtained depending on the ob-
274 jective and risk assessment of the decision-maker represented by the λ parameter, balancing
275 the maximization of the utility function and the protection of the region against the future
276 propagation events (See Appendix, Fig. 10).

277 2.5 Solving scheme

278 Although the problem is NP-hard, being a variant of the maximum-weight connected sub-
279 graph problem (MWCSP), a known NP-hard combinatorial problem (Johnson, 1985), we are
280 able to obtain optimal solutions in all the experiments using a two-stage solving approach.
281 First, we provide a warm-start to the exact MIP model obtained from a greedy algorithm that,
282 given an initial node, selects the adjacent nodes to the current solution with maximum values
283 after sorting them by their $U_i(\lambda)$ until the maximum number of nodes (*Q*) is satisfied. Once
284 the initial feasible solution is provided, we solve the optimization problem with CPLEX
285 v12.9 solver using its default configuration. The two-step solution method approach enables
286 the problem to converge faster because we start the second step with a high-quality feasi-
287 ble solution. This reduces the searching space of the method significantly (upper and lower
288 bounds), improving the convergence and memory usage of the optimization algorithm. Thus,
289 we obtain optimal solutions in reasonable (less than 1 minute on average) solving times in
290 all our experiments. Our solution is guaranteed to be globally optimal because we obtain
291 0% optimality gap solutions from the exact MIP formulation. Although multiple solutions
292 can exist, these are extremely rare in practice.

293 2.6 Case study areas

294 The areas in California selected for the case study are chosen based on factors including
295 significant variation across fuel types, the existence of documented catastrophic fires in the
296 last five years, and the presence of strongly influencing demographic factors. The three areas
297 selected for this study are the Getty center, Napa Valley, and Paradise. Figure 4 denotes the

298 terrain of the three case studies areas. In addition, a summary of the key features of our three
 299 study instances including area, mean elevation, dominating fuel types, and elevation range
 300 are presented in Table 1.

301 **Napa valley.**

302 Napa County, also known as Napa valley is recognized worldwide as a premium wine region.
 303 In addition, the region is also responsible for the production of many agricultural crops.
 304 According to the U.S. Census Bureau, the county has a total land area of about 748 square
 305 miles and a population of 137,744 as of 2019 (Census, 2019). However, this region has
 306 also suffered a number of destructive fire events. A recent article mapping all fires in the
 307 region from 1950 to 2019 shows that the fires have been getting larger and more destructive
 308 (Krishnakumar, 2019). Most notably the 2017 “Tubbs” fire in the Napa and Sonoma counties
 309 is the second most destructive fire recorded in California’s history (Houck and Staff, 2018).
 310 The long fire history experienced by this region coupled with its landscape being suitable
 311 for the farming of different agricultural products particularly grapes from vineyards makes
 312 it a very relevant and interesting area to study in California. The total number of nodes and
 313 edges conforming this instance are 9,309 and 72,272, respectively.

314 **Paradise.**

315 Paradise is a small town located in Butte County in California that has experienced the most
 316 destructive fire in California’s history at the end of 2018. In 2018, the population of Paradise
 317 was about 26,800 with a land area of about 18.31 square miles (Census, 2019; Houck and
 318 Staff, 2018). However, the population numbers after the fire event are unknown as over
 319 9300 were displaced and relocated during and after the fire (Kuruvelia and Lee, 2012). We
 320 use population numbers before the fire as an estimate for our analysis. This town is a unique
 321 region to study because of its high fire risk, limited accessibility to, and relative isolation
 322 from neighboring towns. With a total number of 11,477 nodes and 81,581 edges, it is the
 323 largest instance of the study.

324 **Getty center.** The Getty center, a campus of the Getty Museum and its surrounding regions
 325 located in Los Angeles is selected due to its 2019 fire which forced the museum to temporar-
 326 ily close its doors (Cascone, 2019). This region is different from the other regions of interest
 327 because it is located in an area with a more built-up environment and less vegetation. We
 328 speculate that the demographic factors will have a stronger influence on our analysis of this
 329 region. Modeling the instance as a network, it consists of 5,454 nodes connected by 41,166
 330 edges.

Table 1: Summary of instances’ main characteristics. For each instance, we provide the total area in hectares, the average elevation and its range in meters, the dominant flammable fuel of the terrain following the fuel type layer characterization, the total number of different fuels available in the region, and the number of edges conforming the network used for the optimization model connecting the flammable cells (in any direction).

Instance	Area [ha.]	Mean elev. [m]	Elev. range [m]	Dominant flammable fuel	# Fuel types	# Edges
Napa Valley	9,540	376.74	[131, 724]	SH2 is woody shrubs and shrub litter	16	72,272
Getty center	11,102	221.39	[39, 596]	GS2 is grass and shrubs combined	11	41,166
Paradise	13,433	449.71	[0, 740]	TL6 is moderate load broadleaf litter	17	81,581

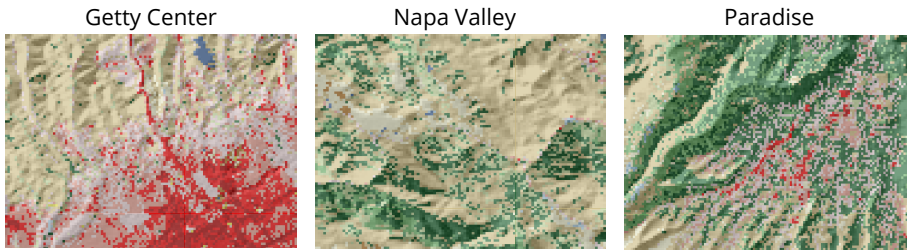


Figure 4: Land cover representations. The three case studies areas are depicted with a hill shade effect where different colors represent the fuel types characterizing the instances following the Scott & Burgan (Scott, 2005) classification system.

331 **Utility Mapping.** For each of the three instances we study, we utilize four layers in our
 332 utility function including forest, volume of carbon sequestered, accessibility, and popula-
 333 tion density layers. We select mapping functions to highlight the priorities of the decision-
 334 maker for every layer. These functions serve to map the values of our current layers to a
 335 range between 0 and 1 using a pre-specified distribution. We Choose an exponential map-
 336 ping function for the population density layer because we want an increasingly high utility
 337 as the number of people in a region increases. In addition, we use the inverse function to
 338 map our accessibility values to the range between 0 and 1. This function is selected to re-
 339 flect increased utility for regions that are closest to densely populated areas. Finally, a linear
 340 function is used to map the volume of carbon sequestered and forest layers to the appropriate
 341 ranges. Our framework allows provides the option to change the distribution of the mapping
 342 functions and customize these functions based on the decision maker's most important con-
 343 siderations. In order to combine the different features into a single utility, we select five
 344 convex combinations of our different layers for our experiments. First, we use an average
 345 combination where all four layers are weighted equally. Then, we create four feature domi-
 346 nant layers, where the selected dominant feature contributes 75% to the final utility whereas
 347 the remaining three layers equally split the remaining. These five utility combinations are
 348 created for each of our three instances (Napa valley, Paradise, and Getty center).

349 2.7 Experiments

350 We model five different NV values for each instance by modifying the μ weights vector as-
 351 sociated with the different four categories following the procedure described in Section 2.3.
 352 In this way, we obtain a balanced weight function $NV_{equal} = \sum_{k \in K} 0.25L_k$ where all layers are
 353 weighted identically and four variations where a dominant layer is weighted by $\mu_{dom} = 0.7$
 354 and $\mu_j = 0.1$ for $j \neq dom \in K$ obtaining $NV_{forest}, NV_{access}, NV_{carbon}$, and $NV_{population}$.

355 A total of $R = 100$ replications with random ignitions and defined D1L1 weather sce-
 356 narios are performed in the simulation module to obtain the final DPV heatmaps using the
 357 previously generated NV values as the node weights, multiplied by $\alpha_i = \text{number of neigh-}$
 358 $bors \text{ connected to node } i$. For each instance and NV value combinations, we generate utilities
 359 $U(\lambda)$ with $\lambda \in \{0, 0.25, 0.5, 0.75, 1\}$. Each combination is then solved in the optimization
 360 module for all treatment levels $tf \in \{0.05, 0.1, 0.15, 0.2, 0.25, 0.5\}$, solving a total of 450 op-
 361 timization problems. Optimal solutions $X^*(\lambda, tf)$ indicating the selected cells are recorded
 362 for each combination.

Finally, we evaluate the average expected losses, $\mathbb{E}[\text{Losses}(X^*(\lambda, tf))]$, due to future wildfire events in each instance, given the output of the resource allocation plan. For this, we estimate the expected damage provoked by future fires – discounted by a $\gamma \in (0, 1]$ factor set to $\gamma = 0.9$ – using $R = 100$ simulations in a modified landscape where the selected cells from the optimal solution of the $ORAP_\lambda(tf)$ model are transformed into non-flammable ones. We use this as a simplified version of a more realistic setting where certain fuel treatment actions (or resource allocation) will decrease the fire susceptibility (or effective ROS) of a certain cell but it will be still flammable. The pseudo-code summarizing all the experimental steps can be found in the Appendix (see Fig. 1).

2.8 Computational implementation

The Cell2Fire fire-growth simulator is implemented in C++ using the boost and omp libraries (Schäling, 2011; Tian et al., 2002) to allow shared memory parallel execution. The decision support system which wraps the simulation module and processes all relevant outputs is programmed in Python. Statistics and visualizations are processed using the known Pandas, Numpy, and Seaborn libraries. Network structures are managed with the networkx package (Hagberg et al., 2013), generating outputs such as propagation trees and providing the users a variety of complex network metrics out-of-the-box such as betweenness centrality for developing their own fire risk indexes. We implement derivative-free optimization algorithms (Conn et al., 2009) in our framework using the NLOPT package (Johnson, 2014). Meta-Heuristics (e.g., genetic algorithms) follow the DEAP (Fortin et al., 2012) library framework. In addition, we rely on the PYOMO modeling language (Hart et al., 2017), a flexible package to generate linear/non-linear models and solve them via an open-source or commercial solver depending on the user needs to embed mathematical programming models in the framework’s optimization module. The utility mapper standalone application and scripts are programmed in Python using the PyQt5 package and compiled using the Pyinstaller package.

Experiments are performed in a daily use laptop with I7-4200 2.1 GHz processor, RAM Memory 8 GB DDR3, and Ubuntu 14.0 OS. All codes are available for public use at <http://www.github.com/cpaismz89/DPV.Utility>.

3 Results and Discussion

The utility functions in our experiments are obtained by combining raster layers as described in Section 2.3 and the different utility combinations are explained in 2.7. We conceive these different combinations to mimic decision-makers having multiple objectives, where one of the goals is more important than the remaining ones in the decision-making process. In Figure 5, we present the utility maps for all proposed combinations of the primary layers for the three instances we explored. We observe that the combinations produce very different heatmaps which we hypothesize will be translated into different optimal treatment decisions.

3.1 Utility and wildfire risk trade-off

DPV values are obtained for all the generated utility heatmaps following Eq. (2) with NV_j representing the value of cell $j \in V$ from the calculated utility layer. Looking at the DPV

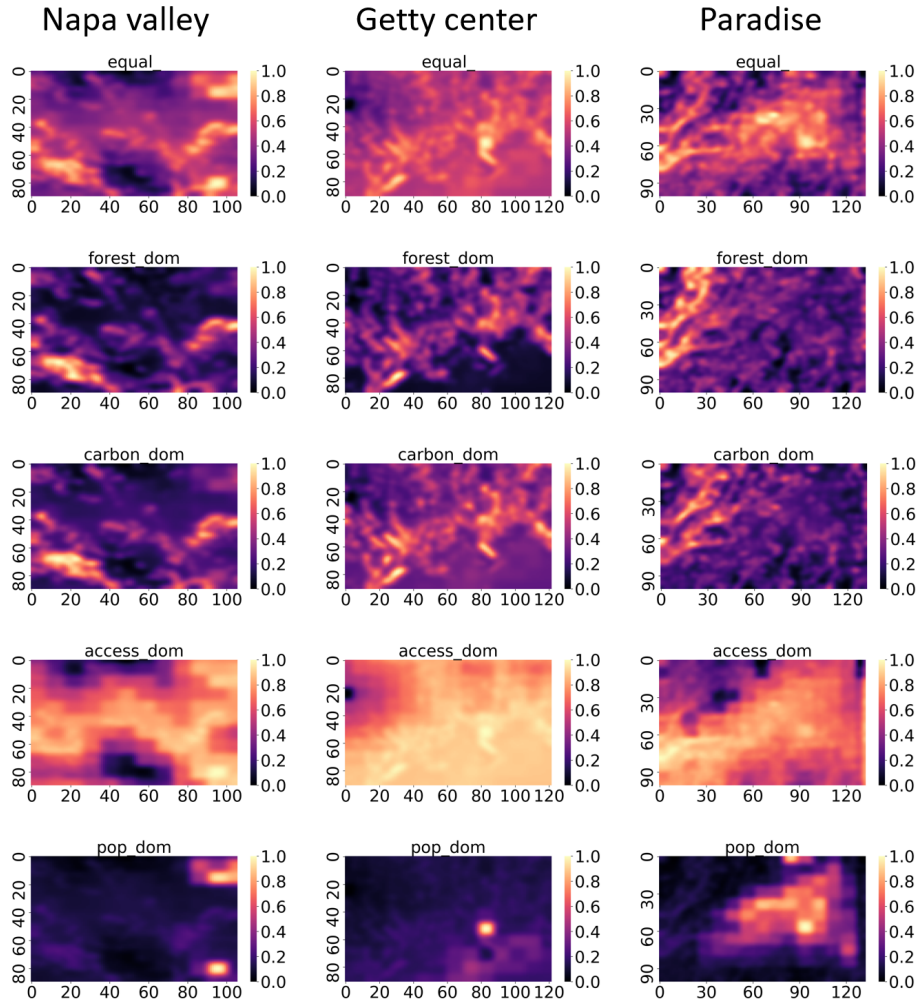


Figure 5: Utility heatmaps for all proposed convex combinations of the main four categories for each instance (columns). The first row represents a balanced combination of all four categories ($\mu_i = 0.25 \forall i$). The suffix *dom* indicates that the dominant category was weighted by $\mu_{dom} = 0.7$ and the remaining three categories with $\mu_j = 0.1, \forall j \neq dom$.

404 matrices (Fig. 6), we clearly observe the most likely wildfire propagation patterns after per-
 405 forming $R = 100$ replications for each instance (first column) where lighter colors highlight
 406 those sections of the landscape with higher DPV, i.e., the nodes that play a fundamental role
 407 in propagating the fire between different areas of the land. As expected, the DPV matrix
 408 obtained for the Napa Valley instance covers a significant portion of the landscape (88.63%)
 409 since it is the one with the largest proportion of flammable fuel types, representing 97.5%
 410 of its total composition. On the other hand, Paradise and Getty center instances include a
 411 significant proportion of non-flammable nodes representing urban settlements/rocky areas

412 (14.56% and 50.87%, respectively) leading to more focused DPV heatmaps surrounding
 413 those areas, covering 40.3% and 37.27% of their total size, respectively.

414 The expected area burned and expected utility losses under the current conditions, i.e.,
 415 when no resource allocation plan is implemented, can be seen in Table 2. From the experi-
 416 ments, we observe a significant impact on the Napa instance with an expected area burned of
 417 2,055 ha. representing 22% of the landscape. This is translated into expected losses close to
 418 20% among all utility functions with respect to the total value available. In the case of Getty
 419 center, we expect a 19% of the area burned due to future wildfire events, with an impact
 420 on the utility functions varying from 14.32% (Forest dominant utility) to 16.18% (Access
 421 dominant utility). Finally, due to the characteristics of the Paradise instance – the distribu-
 422 tion of the non-flammable fuel types – a 7% of the total area of the landscape is expected to
 423 be affected by future wildfire events under the tested conditions, leading to expected losses
 424 between 3.91% (Population layer) to 7.58% (Forest layer).

Table 2: The expected area burned and expected losses for all utility functions as a percentage of the total instance area and the total utility available (heatmaps) per instance, re-
 spectively. Expected values are calculated from $R = 100$ independent wildfire replications,
 weighting all simulations equally, and without any intervention of the landscape.

Instance	$\mathbb{E}[Burned]$ %	$\mathbb{E}[L(U_{Equal})]$ %	$\mathbb{E}[L(U_{Forest})]$ %	$\mathbb{E}[L(U_{Carbon})]$ %	$\mathbb{E}[L(U_{Pop})]$ %	$\mathbb{E}[L(U_{Access})]$ %
Napa Valley	22.08%	20.73%	19.66%	20.06%	18.95%	21.75%
Getty center	18.97%	15.27%	14.32%	14.66%	14.43%	16.18%
Paradise	6.94%	6.33%	7.58%	6.83%	3.91%	6.94%

425 Analyzing the most common fuel types involved in the propagation patterns identified
 426 when calculating the DPV, we observe grass and shrubs combined (GS2, 36.84%), grass
 427 though small amounts of fine dead fuel (GR2, 27.18%), and woody shrubs and shrub litter
 428 (SH7, 20.40%) for Napa Valley; woody shrubs and shrub litter (SH7, 50.73%) and grass and
 429 shrubs combined (GS2, 46.14%) in the area near Getty center; and woody shrubs and shrub
 430 litter (SH7-SH5, 62.49%) and grass and shrubs combined (GS2, 23.14%) for the Paradise
 431 instance. This information allows the decision-maker to gather relevant insights about the
 432 most dangerous sections of the landscape in terms of wildfire risk and identify the set of
 433 potential actions to mitigate their impact when implementing the solution obtained from the
 434 optimal resource allocation plan.

435 3.2 Resource allocation plans

436 As described in Section 2.4, we analyze the trade-off between the expected losses due to
 437 future wildfires in the area after applying the optimal resource allocation plan – assuming
 438 full protection of the selected nodes for simplicity – and the protected value due to the
 439 implementation of this plan by combining the utility layer generated by the decision-maker
 440 and the DPV matrix obtained from the simulations via the λ parameter. Depending on the
 441 expectations of the decision-maker and his/her level of risk aversion, different λ values
 442 should be tested and selected for a particular region and context. In the rest of this section, we
 443 will focus our attention on three interesting results where the trade-off between present value
 444 and future protection plays a crucial role in the decision-making process. This analysis can
 445 be performed for all combinations of utilities, treatment fractions, and instances, providing

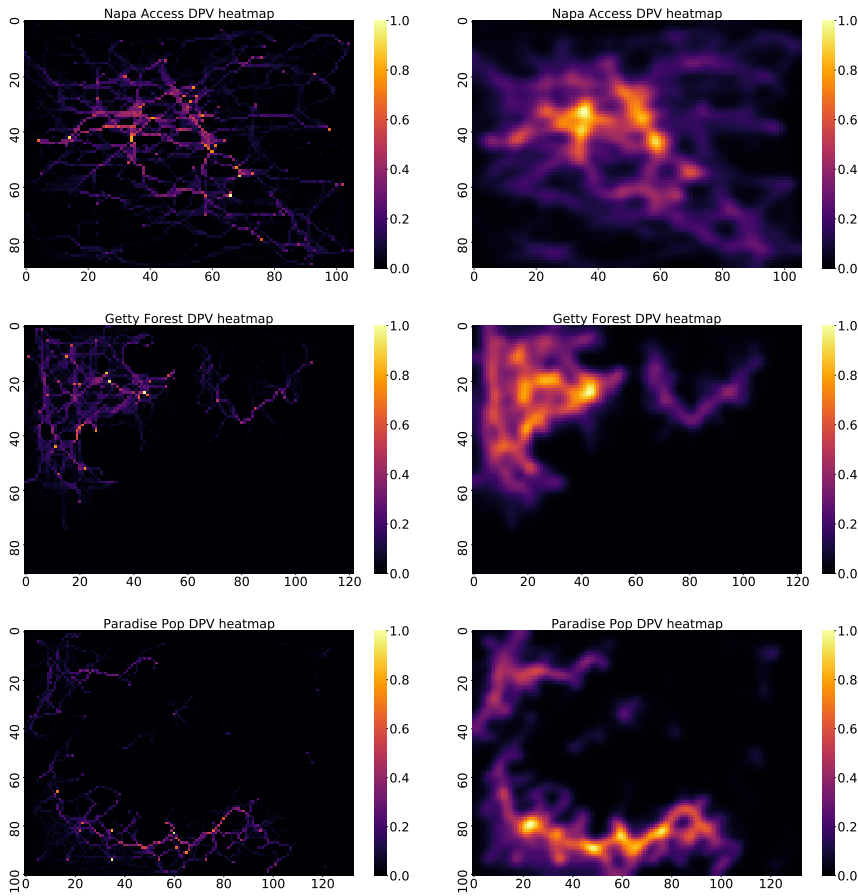


Figure 6: Raw (left) and smoothed (using a Gaussian kernel - right) DPV heatmaps calculated for Napa valley, Getty center, and Paradise instances using the Access, Forest, and Population density layers as the dominant layers for the NV function, respectively. Lighter cells increasingly highlight the nodes playing a fundamental role in propagating the fire to the rest of the landscape.

446 the decision-maker with a comprehensive set of results (see Tables 3, 4, and 5 in Appendix)
 447 and quantitative support for establishing the optimal point to balance the trade-off between
 448 present utility and future protection of the landscape.

449 To illustrate and analyze the inherent trade-off between present utility and the future
 450 protection of the landscape, we observe the results for the Napa valley instance when iden-
 451 tical weights are provided for all categories conforming the utility layer (Fig. 7-(a)) and a
 452 25% of the landscape is protected. As expected, the present/raw utility tends to decrease
 453 as $\lambda \rightarrow 1$ since the decision-maker is sacrificing present utility by focusing more resources
 454 in those locations where the fire will likely propagate, prioritizing the disruption of future
 455 wildfire events instead of the original utility function. However, present utility values are
 456 overestimated when $\lambda \rightarrow 0$ as the decision-maker oversees the impact of future wildfires,

not accounting for this risk. From the graph, we can observe that the best performance in terms of discounted utility is attained when $\lambda = 0.5$ (1017.39 ± 186.06), obtaining the best balance between raw utility and expected wildfire losses using a discount factor of $\gamma = 0.9$.

Analyzing the gaps between the present utility and the discounted function, we observe a clear decreasing pattern as $\lambda \rightarrow 1$ in terms of total utility value variations², with differences of 38.23%, 30.6%, 23.65%, 15.75%, and 7.41 %, respectively. This is aligned with our expectations: as λ is increased, the lands are better prepared for future wildfires, minimizing the gap between today's total utility and the discounted function by sacrificing present value. Looking at the distribution of the discounted utility as a function of λ (Fig. 7-(b)), we observe that increasing the weight of the expected wildfire risk ($\lambda \rightarrow 1$) results in a more compact distribution of the discounted utility $\Delta U(\lambda)$, as seen in the graph. This is consistent with the fact that higher λ values lead to better protection plans by sacrificing the value of the utility function, a trade-off that the decision-maker will analyze to decide which resource allocation plan is aligned with her expectations and goals.

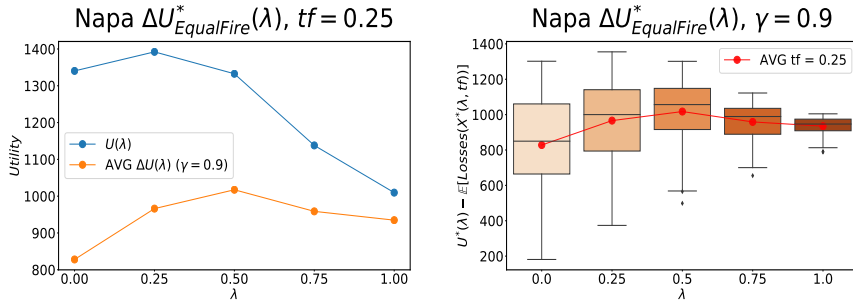


Figure 7: (a) Napa valley instance raw utility (blue) $U(\lambda)$ weighting all categories by identical weights and average discounted utility (orange) $\Delta_{tf}U(\lambda) = U^*(\lambda) - \mathbb{E}[\text{Losses}(X^*(\lambda, tf))]$ including future expected losses due to wildfire events as a function of λ . Treatment fraction is set to 25%. (b) Distribution of the optimal utility discounted by future expected wildfire losses ($\gamma = 0.9$) for different λ levels when protecting 25% of the landscape. Average values are highlighted with red dots.

We then focus our attention on the results obtained for Paradise with a carbon dominated utility when treating 50% of the total landscape. Visualizing the optimal plans for multiple λ values (Appendix, Fig. 10), we observe that the resource allocation plan is not as sensitive as in the case of Napa Valley, but we can still observe differences across the different levels of λ to analyze the trade-off between present value and the protection of the landscape. This is mainly associated with three factors: (1) we are treating 50% of the land so there exists a larger overlap between the optimal plan and the propagation patterns identified in the DPV matrix, (2) the distribution of the carbon dominated utility matches the most relevant DPV spread lines, and (3) the instance, similar to the results from Getty center, presents a significant amount of non-flammable nodes, thus limiting the potential fire spread paths.

This is translated into significantly smaller gaps between the present/raw utility value and the discounted one for all λ levels (3.15%, 2.45%, 0.86%, 0.4%, and 0.04%, respectively). As seen in Fig. 8-(a), both functions converge to an almost identical value for

² Calculated as $\mathbb{E}[\text{Losses}(X^*(\lambda, tf))] / U^*(\lambda, tf)$

484 $\lambda \geq 0.5$. This situation indicates that optimal plans giving at least 50% of weight to the
 485 DPV layer are able to significantly control and mitigate the future expected losses due to
 486 wildfire events. Observing the distribution of the discounted utilities in Fig. 8-(b), it can be
 487 seen that the value and variation in the discounted utility (y-axis) are significantly affected
 488 by λ , obtaining different levels of risk. From the results, the plan obtained when $\lambda = 0.5$
 489 arises as a good solution, balancing the raw utility and expected losses as well as being
 490 characterized by a compact distribution (2250.25 ± 17.58). Values of $\lambda < 0.5$ lead to greater
 491 average discounted utility (red dots) but incur in more risk and potential negative outcomes
 492 (e.g., low discounted utility value outliers in $\lambda = 0.25$). On the other hand, values with
 493 $\lambda > 0.5$ sacrifice a portion of present utility to decrease the impact of expected future losses
 494 (5.1% and 14.5% w.r.t. $\lambda = 0.5$, respectively).

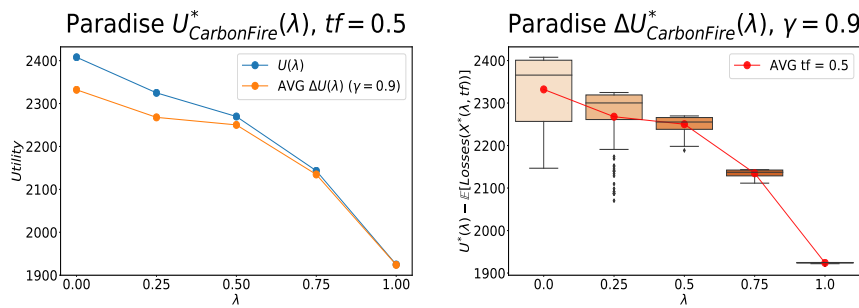


Figure 8: (a) Paradise instance raw utility (blue) $U(\lambda)$ with carbon as the dominant category and average discounted utility (orange) $\Delta_{tf}U(\lambda) = U^*(\lambda) - \mathbb{E}[Losses(X^*(\lambda, tf))]$ including future expected losses due to wildfire events as a function of λ . Treatment fraction is set to 50%. (b) Distribution of the optimal utility discounted by future expected wildfire losses ($\gamma = 0.9$) for different λ levels when protecting 50% of the landscape.

495 Finally, we analyze the results obtained for the Getty center instance, when the utility
 496 function is dominated by the accessibility layer and only 15% of the landscape receives treat-
 497 ment. Contrary to the previous results, we observe an increasing pattern in the discounted
 498 utility (Fig. 9-(a)) as more weight is provided to the DPV matrix, this is, the optimal plan
 499 is mainly aligned with the mitigation of future wildfire losses instead of the current benefit
 500 ($\lambda \rightarrow 1$). These results indicate that, for this particular experiment, focusing the attention
 501 only on the present objective function value for selecting the nodes to be treated/protected
 502 is not the most efficient solution as there is no significant intersection between the treat-
 503 ment plan and the most likely propagation patterns experienced in the landscape, leading
 504 to larger expected losses as $\lambda \rightarrow 0$. Analyzing the gap between both curves, we observe
 505 differences of 148.48%, 119.77%, 74.86%, 49.17%, and 31.64% as we increase the value
 506 of λ , respectively. Therefore, $\lambda = 1$ arises as a robust option under the current experimental
 507 parameters.

508 Following the discussion, we observe how the distributions of the discounted utili-
 509 ties (Fig. 9-(b)) with $\lambda < 0.5$ are particularly wide with a significant bias to the bottom
 510 (-205.64 ± 434.12 and -75.1 ± 364.49 respectively). Even more, we can see that both dis-
 511 tributions reach negative values because of the larger expected losses, indicating higher risk
 512 involved in those treatment plans as they do not prepare the landscape to disrupt future wild-
 513 fire events. Values of $\lambda \geq 0.5$ lead to more compact distributions – still with negative results

514 – by sacrificing valuable outcomes but assuring the future protection of relevant flammable
 515 areas detected by the DPV layer, mitigating the expected losses. This is reflected in the dis-
 516 tribution of the discounted utility when $\lambda = 1$, with an expected discounted utility of 211.05
 517 an a standard deviation of 103.45, contrasting the results above with $\lambda \in \{0, 0.25\}$.

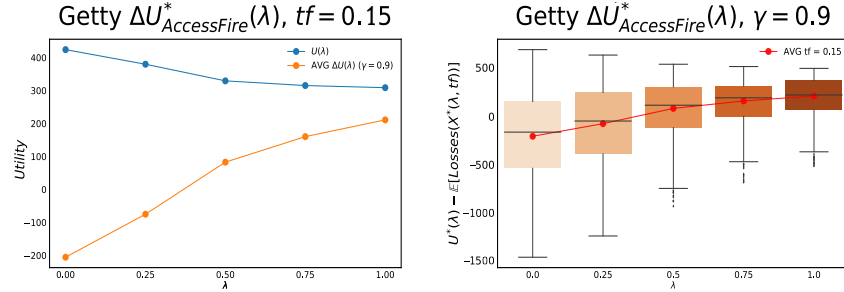


Figure 9: (a) Getty center instance raw utility (blue) $U(\lambda)$ with accessibility as the dominant category and average discounted utility (orange) $\Delta_{tf}U(\lambda) = U^*(\lambda) - \mathbb{E}[\text{Losses}(X^*(\lambda, tf))]$ including future expected losses due to wildfire events as a function of λ . Treatment fraction is set to 15%. (b) Distribution of the optimal utility discounted by future expected wildfire losses ($\gamma = 0.9$) for different λ levels when protecting 15% of landscape.

518 4 Conclusions

519 Decision-makers usually face multiple objectives when making decisions intersecting land-
 520 scape and fire management. In our original approach, the different cells within the landscape
 521 were given equal importance. We extend these previous analyses to include multiple objec-
 522 tives into the optimization model and analyze the trade-off between current weighted objec-
 523 tives and future protection against wildfire risk. Experiments were performed on three dis-
 524 tinct regions using multiple utility functions obtained from the combination of demographic
 525 and environmental raster layers, highlighting different priorities of the decision-maker.

526 The study areas are selected to illustrate the framework when dealing with different
 527 fuel compositions and utility distributions. These differences are reflected in the Napa in-
 528 stance with much higher proportions of flammable fuel types having a more expanded DPV
 529 matrix compared to the other two instances presenting area-focused DPV because they are
 530 composed of higher fractions of non-flammable landscape types. The DPV matrix provides
 531 insight into high-risk areas within the landscape and informs actions to reduce expected
 532 wildfire impacts. Regions with more compact matrices could suggest that fewer resources
 533 are needed to mitigate the effects of future wildfires in these areas. As conjectured from
 534 the calculated DPV, the expected area burned and expected losses for all utility functions as
 535 a percentage of the total instance area and the total utility available (heatmaps) was high-
 536 est in the Napa instance. In addition, we observe that the fuel types commonly involved in
 537 fire propagation patterns consist mainly of some combinations of grass, woody shrubs, and
 538 shrub litter across all three instances.

539 In our analysis, the trade-off between present utility and the future protection of the
 540 landscape based on the DPV is evaluated. As expected, in general, the present utility tends

541 to decrease as λ value rises as the decision-maker increasingly focuses more resources on
542 areas with higher fire spread risk. However, present utility values are overestimated when
543 λ drops, as the decision-maker emphasizes more the impact on the current utility function
544 and less the future wildfire risk. Despite these common trends, certain utility layers present
545 different patterns depending on the instance. For example, we can find that global maximum
546 ΔU values can be obtained with $\lambda = 0$ (e.g., the forest utility layer in Napa) when the
547 most likely propagation patterns are not associated with the highest values of the utility
548 heatmap, reducing the risk at a very high cost of present utility. In other cases, a balanced
549 $\lambda = 0.5$ accounts for a good trade-off between minimizing expected losses and maximizing
550 the present utility as in the Napa U_{Equal} scenario. In addition, some scenarios including
551 certain combinations of utility layers and instances characteristics are harder to balance with
552 future expected losses, mainly due to the fragmentation of the instance and the distribution
553 of the utility layer over the landscape, which can sometimes be too focused on a single point
554 or significantly sparse, focusing the treatment plan on areas that are not likely to match the
555 most relevant propagation patterns of the expected fires.

556 These results suggest that utility functions need to be carefully generated and analyzed
557 by the decision-maker in order to represent his/her expectations and concerns about the
558 landscape because they play a crucial role in generating adequate treatment plans. Moreover,
559 the results presented in this work are conditional upon the occurrence of fires within specific
560 time frames, meaning that the evaluation of the effectiveness of the fuel treatment plans
561 assumes that new wildfires occur during the period of time in which treatments are highly
562 effective. This may not be the case in practice, where the temporal dimension (when to apply
563 the treatment) is crucial to implement effective plans. Some extensions to this work would
564 involve solving a multi-stage version integrating the current framework with forest growth
565 and the inclusion of an explicit multi-criteria optimization model including the generated
566 utility functions as the main objectives, analyzing the trade-off of multiple feasible plans via
567 useful techniques such as Pareto frontiers. In addition, we can incorporate wildfire severity
568 and frequency prediction model into the framework, developing and end-to-end solution for
569 the decision-makers. Another future direction can involve using future projected layer values
570 (e.g., population) as model inputs to consider providing solutions that include projected
571 changes in different demographic and environmental factors of interest.

572 **Conflict of interest**

573 The authors declare that they have no conflict of interest.

574 **Availability of data and material**

575 All data products and sub-products have been recorded and organized into a series of GeoTif
576 files, ready to share with other researchers and the community in an open-source repository
577 (http://www.github.com/cpaismz89/DPV_Utility_Extension) and Google Earth En-
578 gine assets.

579 Code availability

580 The code to reproduce every step of our research is available as a series of Python scripts
581 and Jupyter notebooks for visualization convenience. All code is available at http://www.github.com/cpaismz89/DPV.Utility_Extension.

583 Authors' contributions.

584 C.P. and P.M. designed the research, C.P. developed software, P.M. gathered the data, Z-J.S.
585 guided the research, C.P. and P.M. wrote the manuscript, Z-J.S. edited and supervised the
586 final manuscript.

587 References

- 588 Abatzoglou, J. T. and Williams, A. P. (2016). Impact of anthropogenic climate change on
589 wildfire across western us forests. *Proceedings of the National Academy of Sciences*,
590 113(42):11770–11775.
- 591 Agee, J. K. and Skinner, C. N. (2005). Basic principles of forest fuel reduction treatments.
592 *Forest ecology and management*, 211(1-2):83–96.
- 593 Alcasena, F. J., Ager, A. A., Salis, M., Day, M. A., and Vega-Garcia, C. (2018). Optimizing
594 prescribed fire allocation for managing fire risk in central catalonia. *Science of the total
595 environment*, 621:872–885.
- 596 Baldassari, E. (2018). Camp fire death toll grows to 29, matching 1933 blaze as state's
597 deadliest. *East Bay Times (November 12, 2018)*.
- 598 Barnett, K., Parks, S., Miller, C., and Naughton, H. (2016). Beyond fuel treatment effectiveness:
599 Characterizing interactions between fire and treatments in the us. *Forests*, 7(10):237.
- 600 Birdsey, R. A. (1992). *Carbon storage and accumulation in United States forest ecosystems*,
601 volume 59. US Department of Agriculture, Forest Service.
- 602 Burgan, R. E. (1984). *Behave: fire behavior prediction and fuel modeling system, fuel sub-
603 system*, volume 167. Intermountain Forest and Range Experiment Station, Forest Service,
604 US Department of Agriculture.
- 605 Calviño-Cancela, M., Chas-Amil, M. L., García-Martínez, E. D., and Touza, J. (2016). Wild-
606 fire risk associated with different vegetation types within and outside wildland-urban in-
607 terfaces. *Forest Ecology and Management*, 372:1–9.
- 608 Carrasco, J., Pais, C., Shen, Z.-J. M., and Weintraub, A. (2019). Adjusting rate of spread
609 factors through derivative-free optimization: A new methodology to improve the perfor-
610 mance of forest fire simulators. *arXiv preprint arXiv:1909.05949*.
- 611 Cascone, S. (2019). The getty museum closes its doors as wildfires rage in california, but
612 says the art is safe inside its fireproof building. *Artnet News*.
- 613 Census, B. (2019). U.s. census bureau quickfacts: Napa county, california. *Census Bureau
614 QuickFacts*.
- 615 Chung, W. (2015). Optimizing fuel treatments to reduce wildland fire risk. *Current Forestry
616 Reports*, 1(1):44–51.
- 617 Conn, A. R., Scheinberg, K., and Vicente, L. N. (2009). *Introduction to derivative-free
618 optimization*, volume 8. Siam.

- 619 Conrad, J. M., Gomes, C. P., van Hoeve, W.-J., Sabharwal, A., and Suter, J. F. (2012).
620 Wildlife corridors as a connected subgraph problem. *Journal of Environmental Eco-*
621 *nomics and Management*, 63(1):1–18.
- 622 Curt, T., Fréjaville, T., and Lahaye, S. (2016). Modelling the spatial patterns of ignition
623 causes and fire regime features in southern france: implications for fire prevention policy.
International Journal of Wildland Fire, 25(7):785–796.
- 625 DeWald, S. J., Josiah, S. J., and Erdkamp, R. (2005). *Heating with wood: Producing, har-*
626 *vesting and processing firewood*. Cooperative Extension, Institute of Agriculture and
627 Natural Resources, University of Nebraska-Lincoln.
- 628 Edwards, W. P. (2019). The new normal: Living with wildland fire. *Natural Resources &*
629 *Environment*, 33(3):30–33.
- 630 Finney, M. A. (2001). Design of regular landscape fuel treatment patterns for modifying fire
631 growth and behavior. *Forest Science*, 47(2):219–228.
- 632 Finney, M. A. (2004). Farsite: fire area simulator — model development and evaluation.
633 *Rev. ed. US Dept Agric., ForServ. Res. Pap. RMRS-RP-4*, page 48.
- 634 Flannigan, M. D., Krawchuk, M. A., de Groot, W. J., Wotton, B. M., and Gowman, L. M.
635 (2009). Implications of changing climate for global wildland fire. *International journal*
636 *of wildland fire*, 18(5):483–507.
- 637 Fortin, F.-A., Rainville, F.-M. D., Gardner, M.-A., Parizeau, M., and Gagné, C. (2012).
638 Deap: Evolutionary algorithms made easy. *Journal of Machine Learning Research*,
639 13(Jul):2171–2175.
- 640 Foundation, S. E. (2002). How to weight a tree. *Project SUCCEED-HI: For Students!*
- 641 Fuller, T. (2018). Three weeks after fire, official search for dead is completed.
- 642 Geller, C. (2018). Automated burned area identification in real-time during wildfire events
643 using worldview imagery for the insurance industry. In *Earth Resources and Environ-*
644 *mental Remote Sensing/GIS Applications IX*, volume 10790, page 1079015. International
645 Society for Optics and Photonics.
- 646 Gorelick, N., Hancher, M., Dixon, M., Ilyushchenko, S., Thau, D., and Moore, R. (2017).
647 Google earth engine: Planetary-scale geospatial analysis for everyone. *Remote Sensing*
648 *of Environment*.
- 649 Hagberg, A., Schult, D., Swart, P., Conway, D., Séguin-Charbonneau, L., Ellison, C., Ed-
650 wards, B., and Torrents, J. (2013). Networkx. high productivity software for complex
651 networks. *Webová stránka <https://networkx.lanl.gov/wiki>*.
- 652 Hart, W. E., Laird, C. D., Watson, J.-P., Woodruff, D. L., Hackebeil, G. A., Nicholson, B. L.,
653 and Siirola, J. D. (2017). *Pyomo-optimization modeling in python*, volume 67. Springer.
- 654 Hirsch, K., Kafka, V., Tymstra, C., McAlpine, R., Hawkes, B., Stegehuis, H., Quintilio, S.,
655 Gauthier, S., and Peck, K. (2001). Fire-smart forest management: a pragmatic approach
656 to sustainable forest management in fire-dominated ecosystems. *The Forestry Chronicle*,
657 77(2):357–363.
- 658 Houck, k. and Staff, P. (2018). Top 20 most destructive california wildfires.
- 659 Johnson, D. S. (1985). The np-completeness column: an ongoing guide. *Journal of Algo-*
660 *rithms*, 6(3):434–451.
- 661 Johnson, S. G. (2014). The nlopt nonlinear-optimization package [software].
- 662 Jolly, W. M., Cochrane, M. A., Freeborn, P. H., Holden, Z. A., Brown, T. J., Williamson,
663 G. J., and Bowman, D. M. (2015). Climate-induced variations in global wildfire danger
664 from 1979 to 2013. *Nature communications*, 6:7537.
- 665 Krishnakumar, P. (2019). We mapped every wine country fire. they're larger and more
666 destructive than ever.
- 667 Kuruvila, M. C. and Lee, E. (2012). Paradise fire evacuees starting to return home.

- 668 Matsypura, D., Prokopyev, O. A., and Zahar, A. (2018). Wildfire fuel management: network-
669 based models and optimization of prescribed burning. *European Journal of Operational
670 Research*, 264(2):774–796.
- 671 Nauslar, N. J., Abatzoglou, J. T., and Marsh, P. T. (2018). The 2017 north bay and southern
672 California fires: a case study. *Fire*, 1(1):18.
- 673 Omi, P. N. (2015). Theory and practice of wildland fuels management. *Current Forestry
674 Reports*, 1(2):100–117.
- 675 Pais, C., Carrasco, J., Elimbi, P., and Shen, Z.-J. M. (2020). Downstream protection value:
676 Detecting critical zones for effective fuel-treatment under wildfire risk. *Under R1 in
677 Computers & Operations Research*.
- 678 Pais, C., Carrasco, J., Martell, D. L., Weintraub, A., and Woodruff, D. L. (2019). Cell2fire:
679 A cell based forest fire growth model. *arXiv preprint arXiv:1905.09317*.
- 680 Ramírez, J., Monedero, S., and Buckley, D. (2011). New approaches in fire simulations
681 analysis with wildfire analyst. In *7th International Conference on Forest Fire Research*.
- 682 Rollins, M. G. (2009). Landfire: a nationally consistent vegetation, wildland fire, and fuel
683 assessment. *International Journal of Wildland Fire*, 18(3):235–249.
- 684 Running, S. M. (2006). Is global warming causing more large wildfires? *Science*,
685 313:927–928.
- 686 Russo, L., Russo, P., Evaggelidis, I., and Siettos, C. (2015). Complex network statistics to
687 the design of fire breaks for the control of fire spreading. *Chemical Engineering Trans-
688 actions*.
- 689 Salis, M., Laconi, M., Ager, A. A., Alcasena, F. J., Arca, B., Lozano, O., de Oliveira, A. F.,
690 and Spano, D. (2016). Evaluating alternative fuel treatment strategies to reduce wildfire
691 losses in a mediterranean area. *Forest Ecology and Management*, 368:207–221.
- 692 Schäling, B. (2011). *The boost C++ libraries*. Boris Schäling.
- 693 Scott, J. H. (2005). *Standard fire behavior fuel models: a comprehensive set for use with
694 Rothermel's surface fire spread model*. US Department of Agriculture, Forest Service,
695 Rocky Mountain Research Station.
- 696 Sun, K., Masoudvaziri, N., Szasdi Bardales, F., and Elhami Khorasani, N. (2019). Wildfire
697 spread in wildland urban interface (wui) communities in California: Introducing the urban
698 fuel. *AGUFM*, 2019:NH43C–0950.
- 699 Tian, X., Bik, A., Girkar, M., Grey, P., Saito, H., and Su, E. (2002). Intel® openmp
700 c++/fortran compiler for hyper-threading technology: Implementation and performance.
701 *Intel Technology Journal*, 6(1).
- 702 Tymstra, C., Bryce, R. W., Wotton, B. M., Taylor, S. W., and OB., A. (2010). Development
703 and structure of Prometheus: the Canadian wildland fire growth simulation model. *In-
704 formation Report NOR-X-Edmonton (AB): Natural Resources Canada, Canadian Forest
705 Service, Northern Forestry Centre*, 417:102.
- 706 Waddell, D. R. (1989). Estimating load weights with huber's cubic volume formula: a
707 field trial. *Res. Note. PNW-RN-484. Portland, OR: US Department of Agriculture, Forest
708 Service, Pacific Northwest Research Station*. 12 p, 484.
- 709 Williams, A. P. and Abatzoglou, J. T. (2016). Recent advances and remaining uncertainties
710 in resolving past and future climate effects on global fire activity. *Current Climate Change
711 Reports*, 2(1):1–14.

712 **Appendix**

713 **4.1 Mathematical formulation**

714 Based on the model applied in (Conrad et al., 2012; Pais et al., 2020), the $\bar{\lambda}$ -connected ver-
 715 sion of the optimal resource allocation problem ($ORAP_{\bar{\lambda}}$) can be formulated as the following
 716 Mixed-integer programming (MIP) model:

$$(ORAP_{\bar{\lambda}}) \quad \max \sum_{i \in V} U_i(\bar{\lambda}) = \sum_{i \in V} (\bar{\lambda} DPV(i) + (1 - \bar{\lambda}) NV_i) x_i \quad (3)$$

$$\text{s.t.} \quad z + \sum_{j \in V} y_{(s,j)} = Q \quad (4)$$

$$\sum_{i \in V} \alpha_i \leq 1 \quad (5)$$

$$y_{(s,j)} \leq Q \alpha_j \quad \forall j \in V \quad (6)$$

$$y_{(i,j)} \leq Q x_j \quad \forall (i,j) \in E_s \quad (7)$$

$$\sum_{i \in V: (i,j) \in E_s} y_{(i,j)} = \sum_{l \in V: (j,l) \in \tilde{E}} y_{(j,l)} + x_j \quad \forall j \in V_s \quad (8)$$

$$\sum_{i \in V} b_i x_i = B \quad (9)$$

$$\sum_{i \in V} c_i x_i = C \quad (10)$$

$$x_i, \alpha_i \in \{0, 1\} \quad \forall i \in V \quad (11)$$

$$y_{(i,j)} \in \mathbb{R}^+ \quad \forall (i,j) \in E_s \quad (12)$$

$$z \in \mathbb{R}^+ \quad (13)$$

717 In this formulation, an extra cell s acts as the source of all flow of the network obtaining
 718 a new set of nodes $V_s = V \cup \{s\}$. The source is then connected to each node inside V by a
 719 set of directed edges $E_s = \tilde{E} \cup \{(s,i) \mid i \in V\}$. Flow from the source s is sent to the original
 720 network or absorbed by an auxiliary variable $z \in [0, Q]$ with Q the maximum number of
 721 nodes to be selected (eq. (4)). Adjacency constraints are enforced by eqs. (5)-(8). In eq. (5),
 722 at most one cell $i \in V$ is acting as a link between the source s and the original network using
 723 the binary variable α_i , equal to 1 if the cell i gets the flow from the source. To force the
 724 connectivity of the solution, the remaining cells do not get any flow from the source, setting
 725 those flow variables to zero (eq. (6)). Constraint (7) ensures that cells not included as part of
 726 the solution cannot receive flow from any adjacent node $i \in V$. Flow conservation is modeled
 727 by eq. (8), where each node $i \in V$ with a positive flow consumes one unit of flow and any
 728 remaining one is sent to adjacent cells l if an edge (j,l) exists.

Equations (9)-(10) keep track of the total economic benefit (B) and cost (C) of the optimal resource allocation plan, if provided, to account for extra constraints such as budget restrictions. We force the optimal solution to include the desired amount of cells Q to be selected by adding the following equation:

$$\sum_{i \in V} x_i = Q \quad (14)$$

729 In this way, the optimal connected subgraph S will include exactly Q cells.

730 4.2 Experiments Pseudo-code

Algorithm 1 Experiments Pseudo-code

```

1: procedure EXPERIMENTS
2:   for  $dom \in \{forest, access, carbon, population, equal\}$  do
3:     if  $dom == equal$  then
4:       Calculate  $NV_{dom} = 0.7L_{dom} + \sum_{k \in K: k \neq dom} 0.1L_k$ 
5:     else
6:       Calculate  $NV_{dom} = 0.25 \sum_{k \in K} L_k$ 
7:       Calculate  $DPV(i) = \alpha_i \sum_{j \in T_i} NV(j), \forall i \in V$ 
8:       for  $\lambda \in \{0, 0.25, 0.5, 0.75, 1\}$  do
9:         Calculate utility  $U_i(\lambda) = \lambda DPV(i) + (1 - \lambda)NV(i), \forall i \in V$ 
10:        for  $tf \in \{0.15, 0.25, 0.5\}$  do
11:          Get optimal solution  $X^*(\lambda, tf) \leftarrow \text{Solve}(ORAP_\lambda(tf))$ 
12:          Calculate  $\mathbb{E}[Losses(X^*(\lambda, tf))] \leftarrow \text{Simulation}(X^*(\lambda, tf), R = 100)$ 
13:          Calculate  $\Delta_{tf} U(X^*(\lambda, tf)) := U(X^*(\lambda, tf)) - \gamma \mathbb{E}[Losses(X^*(\lambda, tf))]$ 

```

731 4.3 Detailed results

Table 3: Average discounted utility results for Napa instance evaluated from 100 simulations. Results for all λ combinations between the DPV heatmap and NV layers are presented by dominating utility category (column 1) and treatment fraction level (column 2).

Utility	t_f	$\Delta U(0)$	$\Delta U(0.25)$	$\Delta U(0.5)$	$\Delta U(0.75)$	$\Delta U(1)$
Access	0.05	-630.36 ± 697.47	-719.95 ± 733.02	-212.01 ± 343.35	-2.29 ± 217.35	168.94 ± 123.13
	0.10	-204.23 ± 680.14	-222.66 ± 685.27	275.49 ± 260.19	444.88 ± 165.37	567.69 ± 86.51
	0.15	76.93 ± 725.53	482.08 ± 431.61	731.61 ± 220.05	800.39 ± 151.74	903.39 ± 65.42
	0.20	747.88 ± 539.28	939.52 ± 371.53	1143.22 ± 213.7	1134.43 ± 147.12	1216.88 ± 57.02
	0.25	1218.59 ± 453.58	1373.17 ± 344.61	1533.92 ± 213.11	1552.99 ± 132.53	1508.5 ± 53.91
	0.5	3298.82 ± 198.32	3324.25 ± 169.89	3423.14 ± 99.82	3352.41 ± 42.74	3097.83 ± 13.78
Carbon	0.05	-98.88 ± 264.17	-236.28 ± 369.97	-388.85 ± 298.23	-217.91 ± 196.83	-119.62 ± 146.07
	0.10	126.69 ± 258.7	15.7 ± 339.87	-155.04 ± 217.61	-8.59 ± 137.88	60.61 ± 103.34
	0.15	330.78 ± 231.39	345.71 ± 214.09	172.81 ± 178.55	154.35 ± 118.93	209.04 ± 75.63
	0.20	496.06 ± 199.97	520.36 ± 183.79	438.15 ± 161.36	404.96 ± 109.03	339.83 ± 59.88
	0.25	759.32 ± 167.12	822.89 ± 151.53	715.74 ± 139.45	608.36 ± 79.46	494.92 ± 46.97
	0.5	1661.86 ± 113.59	1623.56 ± 116.32	1559.84 ± 132.09	1533.92 ± 78.67	1170.72 ± 25.24
Equal	0.05	-393.71 ± 441.85	-471.49 ± 519.2	-346.28 ± 325.8	-139.49 ± 204.77	-1.67 ± 132.82
	0.10	-49.04 ± 430.45	-100.32 ± 480.92	19.05 ± 243.76	154.46 ± 151.34	262.15 ± 94.0
	0.15	272.19 ± 389.96	347.36 ± 302.84	356.9 ± 203.05	403.82 ± 135.65	491.04 ± 70.41
	0.20	563.05 ± 337.88	626.91 ± 260.67	692.6 ± 191.55	635.5 ± 129.05	694.99 ± 59.39
	0.25	827.96 ± 284.05	966.14 ± 236.93	1017.39 ± 186.06	958.71 ± 108.22	934.82 ± 52.73
	0.5	2373.07 ± 197.32	2251.69 ± 195.28	2237.53 ± 174.00	2288.82 ± 56.59	1980.16 ± 18.02
Forest	0.05	-29.83 ± 222.46	-151.18 ± 304.25	-367.75 ± 267.31	-267.42 ± 203.46	-181.82 ± 163.4
	0.10	196.82 ± 198.16	51.23 ± 275.67	-198.23 ± 206.55	-71.48 ± 134.11	-11.37 ± 95.93
	0.15	355.85 ± 184.95	231.59 ± 249.27	-38.34 ± 177.71	53.45 ± 107.85	105.97 ± 72.67
	0.20	523.46 ± 165.59	482.76 ± 179.07	242.87 ± 164.76	307.56 ± 107.06	229.7 ± 50.59
	0.25	756.43 ± 156.15	751.86 ± 162.06	573.52 ± 156.47	493.94 ± 78.28	350.95 ± 43.45
	0.5	1437.75 ± 119.00	1485.83 ± 83.09	1366.29 ± 102.55	1244.37 ± 69.88	957.45 ± 25.99
Population	0.05	-54.52 ± 145.67	-122.11 ± 201.67	-215.18 ± 282.34	-202.21 ± 166.13	-154.92 ± 139.03
	0.10	47.22 ± 142.73	10.4 ± 147.42	-7.44 ± 149.98	-82.36 ± 139.5	-40.6 ± 110.42
	0.15	126.16 ± 136.79	129.71 ± 112.21	99.94 ± 121.06	7.84 ± 116.75	48.0 ± 84.91
	0.20	213.52 ± 121.23	213.94 ± 107.48	172.36 ± 125.59	150.56 ± 103.08	185.98 ± 70.19
	0.25	288.26 ± 105.29	285.93 ± 118.84	241.63 ± 125.67	250.5 ± 99.98	273.0 ± 52.72
	0.5	681.34 ± 103.15	645.12 ± 127.37	856.13 ± 30.42	817.33 ± 26.46	748.70 ± 17.05

Table 4: Average discounted utility results for the Paradise instance evaluated from 100 simulations. Results for all λ value combinations between the DPV heatmap and the NV layer are presented by dominating utility category (column 1) and treatment fraction level (column 2).

Utility	<i>tf</i>	$\Delta U(0)$	$\Delta U(0.25)$	$\Delta U(0.5)$	$\Delta U(0.75)$	$\Delta U(1)$
Access	0.05	178.43 \pm 318.39	219.03 \pm 277.09	271.39 \pm 171.98	314.29 \pm 106.98	351.16 \pm 69.99
	0.10	709.31 \pm 257.46	713.05 \pm 247.5	772.21 \pm 135.73	763.92 \pm 94.98	770.0 \pm 65.49
	0.15	1170.32 \pm 257.5	1182.01 \pm 235.67	1236.91 \pm 133.02	1201.7 \pm 94.47	1188.84 \pm 66.45
	0.20	1628.9 \pm 254.39	1647.97 \pm 215.35	1666.09 \pm 131.14	1639.13 \pm 95.41	1585.71 \pm 72.64
	0.25	2074.37 \pm 243.06	2096.7 \pm 200.28	2079.68 \pm 128.94	2046.8 \pm 89.94	1981.67 \pm 74.27
	0.5	4107.38 \pm 142.12	4121.74 \pm 152.96	4139.48 \pm 51.61	3974.30 \pm 15.38	3440.25 \pm 0.93
Carbon	0.05	170.0 \pm 167.37	119.33 \pm 212.13	112.99 \pm 202.85	79.86 \pm 169.74	92.99 \pm 144.35
	0.10	501.83 \pm 154.96	395.71 \pm 203.75	406.94 \pm 205.52	377.67 \pm 163.68	326.32 \pm 146.97
	0.15	880.92 \pm 119.85	829.95 \pm 143.02	749.78 \pm 139.05	621.85 \pm 66.66	594.98 \pm 62.37
	0.20	1136.25 \pm 115.12	1111.82 \pm 140.39	1000.25 \pm 82.06	851.37 \pm 35.68	770.77 \pm 30.33
	0.25	1366.23 \pm 118.15	1322.46 \pm 141.34	1267.54 \pm 79.92	1079.41 \pm 23.32	930.57 \pm 13.21
	0.5	2325.86 \pm 75.56	2263.15 \pm 73.76	2242.70 \pm 17.81	2128.67 \pm 8.69	1917.48 \pm 1.24
Equal	0.05	146.99 \pm 253.0	96.19 \pm 298.17	126.65 \pm 192.1	139.03 \pm 133.54	163.79 \pm 96.69
	0.10	517.53 \pm 254.44	463.82 \pm 299.69	454.8 \pm 188.2	430.92 \pm 131.2	402.6 \pm 97.28
	0.15	869.89 \pm 250.2	814.78 \pm 293.29	846.11 \pm 114.27	716.38 \pm 133.36	658.84 \pm 98.7
	0.20	1338.95 \pm 210.91	1296.81 \pm 237.16	1148.80 \pm 85.11	1026.82 \pm 31.18	906.99 \pm 103.73
	0.25	1740.49 \pm 207.27	1744.59 \pm 192.15	1516.46 \pm 71.49	1302.24 \pm 21.32	1154.24 \pm 107.06
	0.5	3295.83 \pm 103.08	3286.24 \pm 104.47	3190.06 \pm 45.89	2953.84 \pm 13.94	2390.28 \pm 1.29
Forest	0.05	216.81 \pm 202.38	249.91 \pm 204.67	213.87 \pm 184.86	198.49 \pm 157.21	190.93 \pm 134.61
	0.10	683.54 \pm 154.58	694.02 \pm 161.88	624.48 \pm 165.31	545.56 \pm 150.06	479.31 \pm 137.23
	0.15	1024.93 \pm 150.04	1017.27 \pm 141.46	990.61 \pm 110.4	848.03 \pm 62.04	778.14 \pm 56.25
	0.20	1298.57 \pm 148.71	1296.31 \pm 142.27	1250.72 \pm 69.61	1115.27 \pm 37.33	991.0 \pm 28.6
	0.25	1528.34 \pm 140.52	1562.9 \pm 106.9	1500.39 \pm 60.08	1395.67 \pm 31.94	1192.01 \pm 12.08
	0.5	2598.65 \pm 64.54	2566.28 \pm 63.29	2551.14 \pm 17.53	2452.89 \pm 8.03	2296.49 \pm 0.90
Population	0.05	324.29 \pm 70.44	268.57 \pm 125.4	-26.16 \pm 106.26	-12.03 \pm 91.99	-0.25 \pm 86.53
	0.10	695.32 \pm 71.5	630.53 \pm 129.06	354.47 \pm 104.33	91.32 \pm 87.87	93.99 \pm 82.53
	0.15	955.1 \pm 73.52	889.47 \pm 127.92	707.54 \pm 105.29	183.65 \pm 88.69	173.49 \pm 85.17
	0.20	1164.93 \pm 72.59	1101.32 \pm 123.66	928.23 \pm 102.43	418.05 \pm 93.16	241.01 \pm 90.85
	0.25	1333.8 \pm 69.21	1279.45 \pm 69.42	1106.89 \pm 103.3	811.5 \pm 93.61	319.53 \pm 93.13
	0.5	2007.73 \pm 35.38	1958.83 \pm 62.23	1852.77 \pm 114.98	1741.65 \pm 78.41	708.24 \pm 3.74

Table 5: Average discounted utility results for the Getty center instance evaluated from 100 simulations. Results for all λ value combinations between the DPV heatmap and the NV layer are presented by dominating utility category (column 1) and treatment fraction level (column 2).

Utility	t_f	$\Delta U(0)$	$\Delta U(0.25)$	$\Delta U(0.5)$	$\Delta U(0.75)$	$\Delta U(1)$
Access	0.05	-472.96 \pm 453.7	-392.1 \pm 417.92	-262.43 \pm 303.32	-139.59 \pm 230.58	-80.92 \pm 201.81
	0.10	-353.71 \pm 443.07	-227.01 \pm 375.65	-72.71 \pm 266.06	4.14 \pm 189.54	69.61 \pm 150.55
	0.15	-205.64 \pm 434.12	-75.1 \pm 364.49	82.81 \pm 213.83	160.22 \pm 136.52	211.05 \pm 103.45
	0.20	-64.41 \pm 431.02	82.69 \pm 350.25	225.15 \pm 184.66	284.95 \pm 120.86	330.84 \pm 74.25
	0.25	125.28 \pm 407.03	211.91 \pm 338.75	355.09 \pm 159.94	406.88 \pm 97.7	445.96 \pm 51.63
	0.5	905.18 \pm 291.65	949.64 \pm 256.68	971.89 \pm 138.03	967.81 \pm 70.83	988.54 \pm 24.95
Carbon	0.05	-205.02 \pm 215.85	-252.35 \pm 283.41	-250.66 \pm 255.97	-177.37 \pm 220.13	-151.03 \pm 213.97
	0.10	-95.77 \pm 205.28	-131.89 \pm 259.1	-85.9 \pm 175.91	-83.15 \pm 171.28	-47.19 \pm 142.25
	0.15	10.27 \pm 191.77	-48.71 \pm 245.27	7.7 \pm 146.14	33.27 \pm 111.25	50.12 \pm 103.33
	0.20	106.72 \pm 176.78	51.74 \pm 222.78	112.5 \pm 140.3	104.59 \pm 82.4	114.97 \pm 82.65
	0.25	183.74 \pm 174.64	121.02 \pm 217.3	187.24 \pm 118.38	170.12 \pm 69.47	178.04 \pm 51.78
	0.5	578.29 \pm 149.24	569.52 \pm 136.31	514.78 \pm 94.54	492.50 \pm 48.50	467.99 \pm 28.17
Equal	0.05	-291.81 \pm 270.13	-340.11 \pm 348.64	-267.66 \pm 274.53	-156.46 \pm 214.39	-121.35 \pm 200.53
	0.10	-182.42 \pm 264.34	-238.24 \pm 329.64	-127.19 \pm 229.6	-52.0 \pm 168.74	-18.22 \pm 153.08
	0.15	-77.81 \pm 262.55	-137.06 \pm 321.14	10.99 \pm 165.64	64.96 \pm 117.05	82.66 \pm 107.17
	0.20	11.86 \pm 255.07	-37.58 \pm 311.16	96.22 \pm 150.43	146.98 \pm 100.09	170.95 \pm 82.78
	0.25	96.76 \pm 246.77	31.2 \pm 307.0	203.37 \pm 136.78	225.95 \pm 82.37	244.5 \pm 52.99
	0.5	636.70 \pm 186.57	633.69 \pm 165.57	589.46 \pm 112.89	600.49 \pm 54.09	599.59 \pm 26.80
Forest	0.05	-154.77 \pm 168.04	-216.76 \pm 232.17	-285.57 \pm 288.36	-226.0 \pm 244.0	-164.97 \pm 214.63
	0.10	-56.82 \pm 156.05	-114.55 \pm 208.5	-133.43 \pm 205.9	-115.09 \pm 178.6	-72.47 \pm 144.47
	0.15	19.91 \pm 144.58	-26.92 \pm 189.24	-45.63 \pm 158.45	-11.54 \pm 119.47	15.09 \pm 103.73
	0.20	96.95 \pm 133.05	36.43 \pm 176.55	38.2 \pm 128.73	48.1 \pm 96.83	67.37 \pm 77.59
	0.25	147.82 \pm 131.6	110.52 \pm 165.47	115.68 \pm 120.95	108.12 \pm 77.0	125.16 \pm 53.59
	0.5	474.79 \pm 99.54	474.01 \pm 102.52	390.05 \pm 94.46	369.58 \pm 54.05	359.10 \pm 28.73
Population	0.05	-70.86 \pm 65.58	-112.05 \pm 109.7	-193.76 \pm 204.4	-173.36 \pm 196.66	-170.81 \pm 198.96
	0.10	-43.46 \pm 64.26	-70.31 \pm 89.42	-136.47 \pm 160.56	-115.5 \pm 150.06	-112.4 \pm 151.19
	0.15	-16.44 \pm 64.65	-27.52 \pm 66.72	-75.13 \pm 113.62	-59.41 \pm 105.36	-56.56 \pm 105.75
	0.20	7.38 \pm 61.85	-4.0 \pm 59.09	-38.04 \pm 93.7	-21.94 \pm 85.87	-19.29 \pm 84.26
	0.25	35.15 \pm 59.66	22.34 \pm 55.45	-2.93 \pm 74.14	14.77 \pm 55.57	18.24 \pm 53.49
	0.5	158.55 \pm 43.87	123.64 \pm 43.91	106.78 \pm 48.59	119.83 \pm 32.95	123.32 \pm 28.41

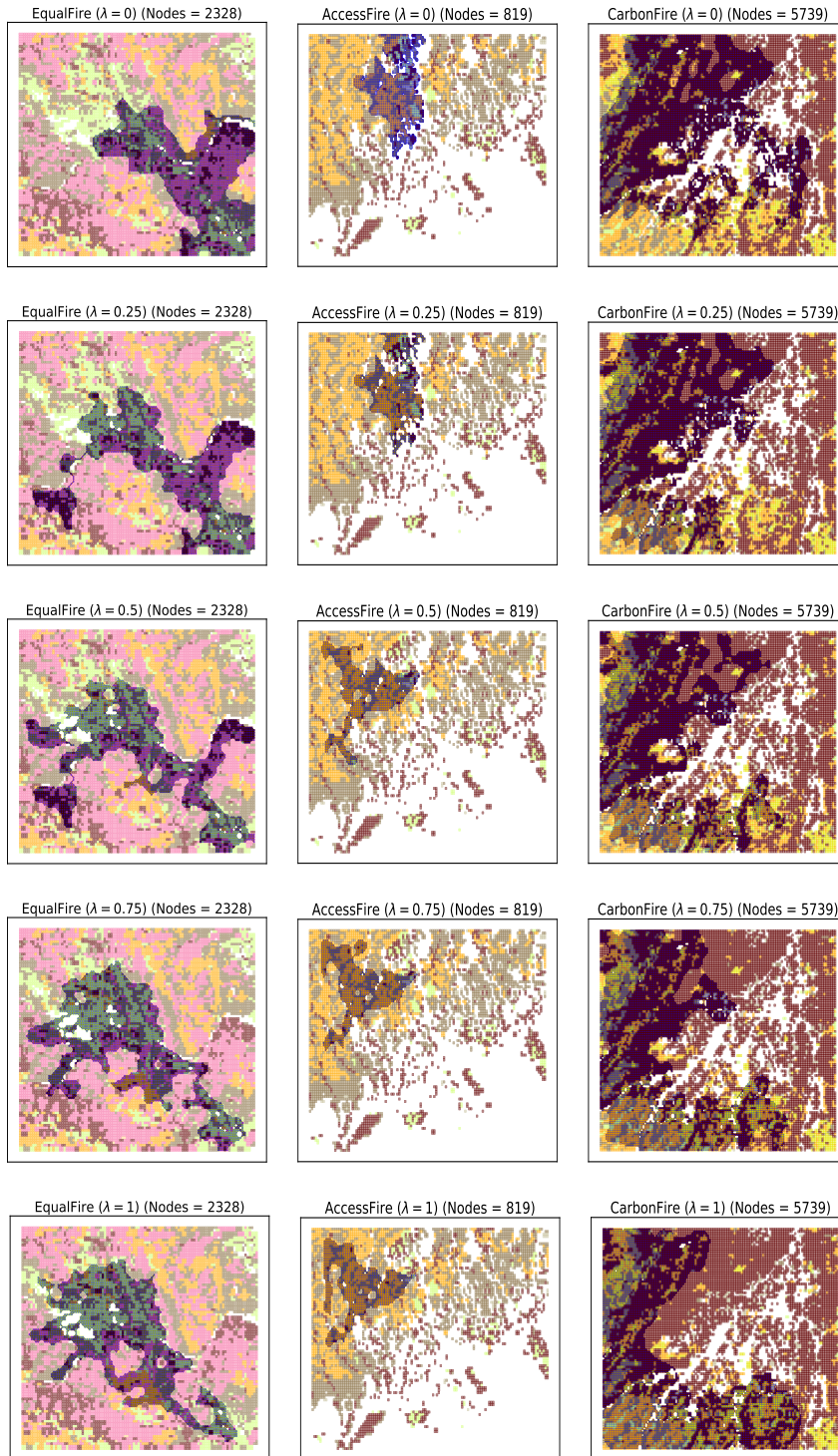


Figure 10: Resource allocation sample plans for Napa valley, Getty center, and Paradise (columns) instances for different λ weights (rows) to account for the expected losses due to future wildfires, at a specific treatment fraction tf . Significant variations in the optimal plans can be observed as the λ values are modified to include future wildfire risk into the objective function. Original land cover colors have been modified for better contrast and non-flammable nodes have been removed (white space).